PRIFYSGOL ABERYSTWYTH UNIVERSITY

Quantitative Measurement of Photo-luminescent Materials.

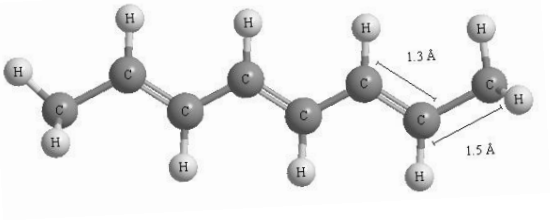

Polyacetylene: a conjugated polymer
Pic Credit: Texas A&M university

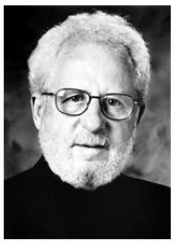

Alan J. Heeger

Alan G. MacDiarmid

Hideki Shirakawa

Jointly Awarded the Nobel Prize in Chemistry in 2000 for the discovery and development of conductive polymers. Credit: Nobelprize.org

By: John Tomes (jjt10@aber.ac.uk)

Abstract:

A review of the literature relating to quantitative measurements of quantum yield for some thin film semiconductor materials. A brief description of the theory of quantum yield and the best method for determining absolute values for thin film materials. Why this is relevant to modern photo-luminescent materials. Detailed explanation of the proposed experiment design, calibration and data acquisition method.

Contents

1. Introduction

The prospect of manufacturing low cost low energy easily assembled and even flexible optoelectronic devices is a key driver for the development of organic thin film semiconductor technology.

The object of this project is to quantify the photo-luminescent properties of some novel conjugated polymer thin film materials.

Conjugated polymers are organic macromolecules that have a spine of alternating single and double bonds. The π-electrons can be preferentially moved from one bond to the other allowing their use as a one dimensional semiconductor. Like inorganic semiconductors they can be doped to control their conductivity. Alan Heeger, Alan MacDiarmid and Hideki Shirakawa received the Nobel Prize for chemistry in 2000 for the discovery and development of conductive polymers.

One of the key parameters that characterises this type of material is its Photo-luminescent Quantum Yield (PLQY). Put most simply the PLQY is the ratio of emitted light compared to absorbed light. This simple ratio is a very powerful tool to define the photophysics of electronic transitions within the material and as a measure of its usefulness in potential applications. The quantum efficiency of photoluminescence is considered to set the upper limit of efficiency of electroluminescent diodes [9].

Electroluminescence is the basis for many types of visual display unit [2,4]. Conjugated polymers offer a robust structure which can be made soluble in organic solvent, allowing fabrication by methods similar to screen or inkjet printing, onto a relatively large area light emitting diode display [3,4]. The advantages of this type of organic light emitting diode (OLED) displays are reduced power consumption, high contrast and low material costs. Active matrix organic light emitting diodes (AMOLED) are a further development and are currently in use on some mobile phone display devices. This uses an active matrix of OLED pixels deposited onto a thin film transistor (TFT) backing which acts as the switching mechanism to control current output to each pixel. This approach offers the possibility of even lower power consumption and lower cost.

For display devices a high PLQY reduces energy consumption requirements. For photovoltaic cells a low PLQY material will be desirable.[3].

Luminescence in conjugated polymers is the result of radiative decay of singlet excitations [5] non radiative processes within the molecule such as structural and conformational relaxation, quenching and electronic energy transfer reduce the efficiency of luminescence [6].

The radiative PLQY (Φ) can be defined as:

$$\Phi = \frac{Number\ of\ photons\ emitted}{Number\ of\ photons\ absorbed} \qquad (1.1)$$

The procedure for establishing the PLQY of materials in solution is relatively straight forward because the emission from the liquid is (accurately) assumed to be isotropic in all directions. Commercial spectroflourimeters make use of this fundamental feature. Measurement of PLQY of thin films is more complex partly due to the fact that for polymeric materials an anisotropy in the chromophores leads to a similar anisotropy in the di-pole moments, additionally they are a high refractive index material and this results in significant waveguiding of the luminescence [1,5].

To account for the anisotropic distribution of the emission an integrating sphere can be used. The purpose of an integrating sphere is to spatially integrate radiant flux. Details of how this is achieved is covered in section 3.

To obtain absolute PLQY values careful calibration to a known standard is required, details of how this can be achieved is covered in section 5.

2. Quantum Yield

2.1 Introduction

One of the key parameters that characterises Conjugated Polymers is its Photo-luminescent Quantum Yield (PLQY). Put most simply the PLQY is the ratio of emitted light compared to absorbed light. This simple ratio is a very powerful tool to define the photophysics of electronic transitions within the material and as a measure of its usefulness in potential applications. The quantum efficiency of photoluminescence (PL) is considered to set the upper limit of efficiency of electroluminescent (EL) diodes in that EL ≈ 25% of PL [9] which has a direct influence on the energy efficiency of opto-luminescent devices.

2.2 How does it characterise a material.

The evaluation of PLQY can provide a direct correlation to the usefulness of a material as a fluorophore in bio-sensing, bio-analysis, fluorescence imaging and opto-electronic applications [19]. A high PLQY is desirable in optical display devices, as low energy consumption is required in most applications. By contrast for materials used in solar cell construction a low PLQY would be preferred as it will improve the quantum efficiency in converting any incoming photo-excitation to electron production.

2.3 The Radiative Process.

As described by Crosby et al and Shuai et al [9,13] a practical organic conjugated polymer light emitting diode (OLED) consists of a number of organic conjugated polymer (OCP) layers sandwiched between an anode and a cathode. Electrons and holes are injected into the polymer layers from these electrodes, the charge carriers then migrate through the OCP usually via inter-chain hopping processes. These then form intrachain excitons. The radiative decay of the singlet excitons produces the observed luminescence.

This and the associated processes are shown in fig 2.1. The radiative decay of singlet excitons is shown as S_1 to S_0, competing non-radiative processes absorb energy in alternative decay processes. With reference to the figure:

Quantum Yield of singlet fluorescence

$$\Phi_f = k_f / (k_f + k_{qf} + k_{is}) \qquad (2.1)$$

Quantum Yield of triplet phosphorescence

$$\Phi_p = k_p / (k_p + k_{qp}) \qquad (2.2)$$

Quantum Yield of inter system crossing

$$\Phi_{is} = k_{is} / (k_{is} + k_f + k_{qf}) \qquad (2.3)$$

The total measured Quantum Yield is:

$$\Phi_{Tot} = \Phi_f + \Phi_p \qquad (2.4)$$

Fig 2.1

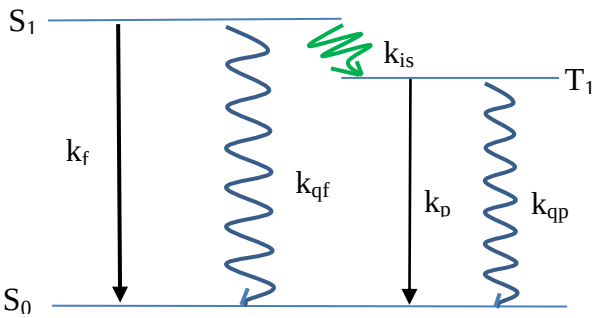

Most aromatic molecules have an even number of π-electrons this results in a ground singlet electronic state S_0 where the electron spins are paired. The excited π electronic states are either singlet S_1 etc or triplet T_1 etc. [14].

In practice the means by which this process is achieved is by conduction through the conjugated polymer.

2.4 Conjugated Polymers

Conjugated polymers are organic macromolecules that have a spine of alternating single and double bonds. The π-electrons can be preferentially moved from one bond to the other allowing their use as a one dimensional semiconductor. Like inorganic semiconductors they can be doped to control their conductivity. Alan

Heeger, Alan MacDiarmid and Hideki Shirakawa received the Nobel Prize for chemistry in 2000 for the discovery and development of conductive polymers

2.5 Methodology

To establish the PLQY of film materials as stated earlier requires consideration of a number of factors, including the anisotropic distribution of the emission, the method of illumination of the sample and a suitable means of gathering the samples emission. The method of Greenham et al utilised a argon-ion laser as an illumination source and an integrating sphere to account for the angular anisotropy. Their method also considers the reabsorption of laser light as a result of secondary reflections that this method introduces. The amount of this secondary absorption is calculated by measurement of the luminescence with the sample not directly illuminated by the laser source [5].

This method was developed further by deMello et al [1] and is considered the basis by which this project will proceed.

Three experimental setups are shown in fig 2.2. The detected luminosity of the illuminating laser light is shown in fig 2.3, the y axis is intensity multiplied by wavelength and thereby proportional to the number of photons within the wavelength interval.

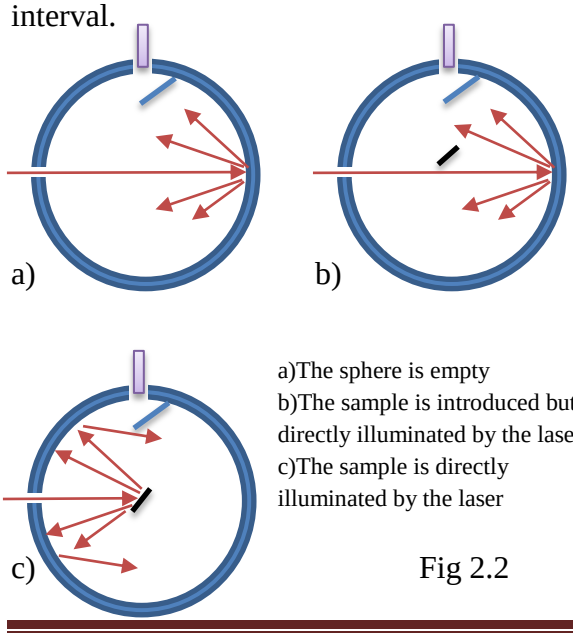

a)The sphere is empty
b)The sample is introduced but not directly illuminated by the laser,
c)The sample is directly illuminated by the laser

Fig 2.2

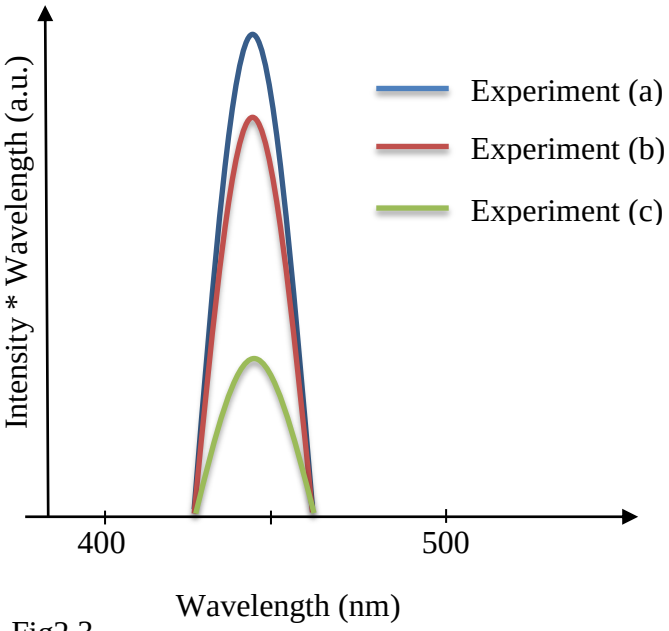

Fig2.3

In each of the experiments the area under the curves shown in fig 2.3 is proportional to the amount of unabsorbed laser light.

In experiment (c) a fraction *A* of the incident laser light is absorbed by the sample, the remaining fraction (1-*A*) will be scattered to the walls of the sphere. A further fraction of this scattered light (μ) will be reabsorbed by the whole surface of the sample. Taking *La*, *Lb* and *Lc* to be the areas under the laser illumination profile for each experiment respectively, equations 2.5 and 2.6 can be derived.

$$L_b = L_a * (1 - \mu) \qquad (2.5)$$

$$L_c = L_a * (1 - A) * (1 - \mu) \qquad (2.6)$$

From (2.5) and (2.6) an expression for the absorption coefficient *A* can be obtained:

$$A = \left(1 - \frac{L_c}{L_b}\right) \qquad (2.7)$$

In Fig 2.4 an approximation of the anticipated emission spectra is shown for both experiments (b) and (c). As before the areas under the emission profile is proportional to the amount of emitted light. Taking these values to be *Eb* and *Ec* respectively it can be determined that,

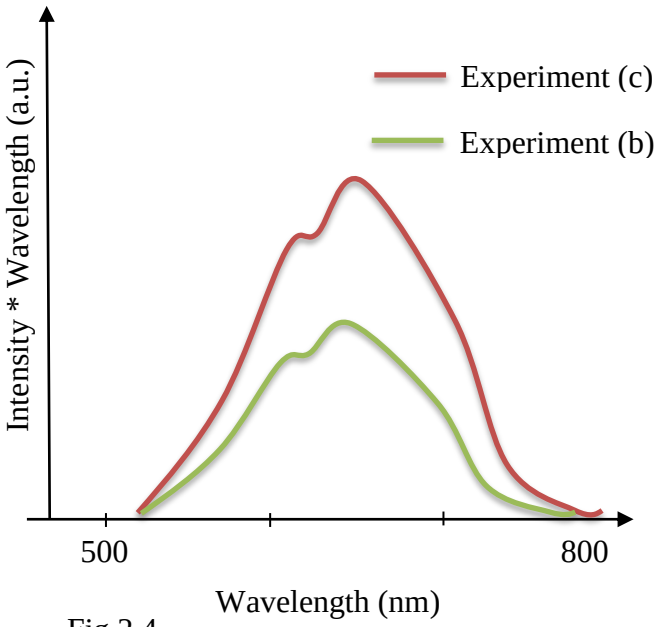

Fig 2.4

the total light incident on the detector is composed of both unabsorbed laser light and emission from the sample.
In experiment (b) this detected light is composed of $L_b + E_b$
In experiment (c) the fraction *A* of the laser light is absorbed leaving (1-*A*) reflected, the contribution of the scattered light to the detected total can then be defined as:

$$(1 - A)(L_b + E_b) \qquad (2.8)$$

The emission from the sample due to the excitation of the laser light is :

$$\Phi L_a A \qquad (2.9)$$

Where Φ is the Quantum Yield (QY). This also contributes to the total measured spectrum, so with consideration of all the contributing factors the total intensity measured over the whole spectrum is given by eqn (2.10)

$$L_c + E_c = (1 - A) * (L_b + E_b) + \Phi L_a A \qquad (2.10)$$

This can then be rearranged for quantum yield substituting eqn (2.7)

$$\Phi = \frac{E_c - (1-A) * E_b}{L_a A} \qquad (2.11)$$

With:

$$A = \frac{L_b - L_c}{L_b} \qquad (2.12)$$

The reabsorption of emitted light from the sample excitation is unavoidable in using an integrated sphere and this factor is not accounted for in the final equation. This should not be a problem if absorption and emission spectra do not overlap but for new materials this cannot be assumed to be the case. Improvement over previous work to minimise this effect could be achieved by incorporating laser alignment features into the sphere to enable reduction of the sample size to just over the collimated beam size. The sample holder could allow rotation to remove the sample from direct illumination, rather than repositioning of the laser source.
A more rigorous mathematical method for the consideration of reabsorption is given by Ahn et al [10] Whereby the observed PLQY is given by a series of successive absorption reemission cycles:

$$\Phi_{obs} = \Phi(1 - a)(1 + a\Phi + a^2\,\Phi^2 + \cdots)$$

Where a = self-absorption parameter dependent on the overlap between absorption and emission spectra.
Such that:

$$a = \int_0^\infty f(\lambda)\left[1 - 10^{-A(\lambda)}\right] d\lambda \qquad (2.13)$$

Where: f (λ) = photons per wavelength interval (normalised to 1)
A(λ) = Absorbance dependent on the extinction coefficient ε(λ) concentration C and distance *x* through which the photons must travel. Described by the Beer-Lambert Law: $A(\lambda) = \varepsilon(\lambda)[C]x$
The culmination of this approach is the final expression:

$$\Phi = \frac{\Phi_{obs}}{1-a+a\Phi_{obs}} \qquad (2.14)$$

This is in contrast to the method of deMello et al which would result in:

$$\Phi = \frac{\Phi_{obs}}{1-a} \qquad (2.15)$$

The deMello approach potentially results in a PLQY value capable of exceeding 100%.

In practice the data collection method of Ahn et al is the same as that of deMello et al. The subsequent mathematical treatment requires the calculation of the value *a* using equation (2.13) plus the Beer-Lambert Law, and a value for *x* from film thickness. Comparison is made to the values obtained directly from analysis of the integrating sphere data. Significantly these values are in good agreement when multiplied by an empirical factor of 20. Ahn et al speculate this is a direct function of the round trips within the sphere and other internal influences. That this multiplication factor is similar to the typical sphere multiplier (3.7) described in the next section is worthy of further investigation. To proceed as per Ahn et al it is necessary to know the un-attenuated emission line shape. In this project that would be best achieved by independent measurement of an ultra-thin sample where self-absorption was not an issue. Cross correlation with the pre-calculated sphere multiplier may well provide further support for the Ahn method and possibly a more rigorous explanation of their empirical factor.

2.6 Comparison to a Known Standard

To confirm that system calibration and data collection methods are valid (discussed in section 5) it is proposed to test a standard solution of Rhodamine in-line with the procedure used by deMello et al and Porres et al [1,6] as literature values for PLQY of Rhodamine are readily available to a good degree of accuracy [19].

3. Integrating Spheres

3.1 Introduction.

The purpose of an integrating sphere is to spatially integrate radiant flux. They are hollow spheres coated internally with a highly diffusely reflecting material. When a light source is placed inside the sphere the light output is redistributed isotropically over the whole of the internal surface despite any angular preference of the initial emission [1,5,10]. The anisotropic angular emission from CPTF materials makes the use of an integrating sphere ideal as a way of collecting data on the total radiative emission of the sample.

3.2 How they Work.

The principal of an integrating sphere stems from the theory of radiation exchange within an enclosure of diffuse surfaces.

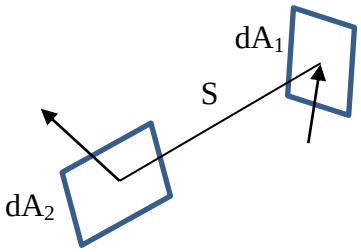

Fig 3.1

The fraction of radiant energy leaving dA_1 and arriving at dA_2 is known as the exchange factor.

$$dF_{d1-d2} = \frac{cos\theta_1 cos\theta_2}{\pi S^2} dA_2 \qquad (3.1)$$

Applying this to the interior of a sphere

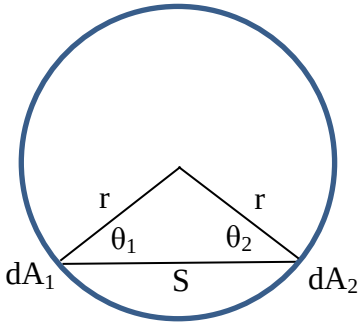

Fig 3.2

Since the distance S = 2r cos θ_1 = 2r cos θ_2

$$dF_{d1-d2} = \frac{dA_2}{4\pi r^2} \qquad (3.2)$$

This equation holds independently of angle or distance between areas as aresult of the inherent geometry of a sphere. The fundamental significance being that the fraction of flux falling on area dA_2 is the same for any point on the spheres internal surface.

If the area dA_1 exchanges radiation with the area A_2 then eqn (3.2) becomes:

$$dF_{d1-d2} = \frac{1}{4\pi r^2}\int_0^{A_2} dA_2 = \frac{A_2}{4\pi r^2} \qquad (3.3)$$

Significantly this is also independent of dA_1

$$F_{1-2} = \frac{A_2}{4\pi r^2} = \frac{A_2}{A_{Sph}} \qquad (3.4)$$

Where A_{sph} is the total internal area of the sphere. As a result, the fraction of radiant flux received by the surface area A_2 is simply the fraction of area it displaces within the sphere.

The radiance of an internally illuminated integrating sphere can be defined as:

$$L = \frac{\Theta_i}{\pi A_s} * \frac{\rho(1-f)}{1-\rho(1-f)} \qquad (3.5)[15]$$

Where: L = radiance, Φ_i= input flux
A_s = Sphere internal area, f = any port area of the sphere which is non-reflecting,
ρ = the reflectance of the material coating the inside of the sphere.

Inspecting eqn (3.5) it can be seen that radiance falls linearly as the area of the sphere increases, however that area is a function of the radius squared.

$$A_s = 4\pi r^2 \qquad (3.6)$$

It is important then to maximise the incident flux on any detector collecting data from the sphere by minimising the sphere diameter. However a trade-off must be made to ensure that the non-reflective areas (f) do not unduly influence the

sphere performance. Equation (3.5) is purposely divided into two parts, the first is the radiance of a diffuse surface. The second part is a quantity known as *M* the sphere multiplier.

$$M = \frac{\rho(1-f)}{1-\rho(1-f)} \qquad (3.7)$$

This factor accounts for the multiple reflections within the sphere which increase the radiance within any given area. In fig 3.3 the graphs show the relation between the sphere multiplier *M* and non-reflective areas f , and surface reflectance ρ.

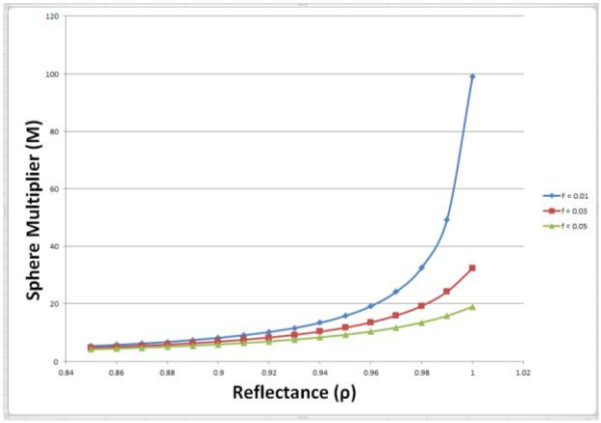

Fig 3.3

It might be thought that the flux density arriving at a detector might be the input flux divided by the total area of the sphere, however the sphere multiplier means that the radiance within the sphere is at least an order of magnitude greater than the simple division of area might suggest. Most commercial Integrating Spheres have a multiplier in the range of 10-30 [15]

3.3 Design guides.

As can be seen from eqn (3.7) it is important to maximise the reflectance value of the coating applied to the internal surface of the sphere and minimise any non-reflective areas. To maintain maximum radiant flux on the detector the sphere should be small but this conflicts with both the effective spatial integration and the fraction of non-reflective surface caused by the need for a suitable port to allow insertion of the sample, the excitation laser aperture and the detector aperture. From eqn (3.5)

3.3.1 Diameter

Calculation of the optimum sphere diameter can be done by initial consideration of the port size and the desire to keep the value of the fraction of non-reflective surface (f) below 5%. Then from eqn (3.5) it can be seen that the surface radiance for an equivalent input flux is proportional to:

$$L_s = \frac{M}{D_s^2} \qquad (3.8)$$

By combination of the input illumination flux, the internal coating reflectance and the photo detector field of view it is possible to calculate for any chosen sphere diameter the incident flux at the detector and ensure it is within the optimum range of the detector.

3.3.2 Coatings

An ideal coating for integrating spheres would be non-specular, high in reflectance and spectrally flat over a wide wavelength range.

As can be seen from fig 3.3 the multiplication factor is heavily dependent on the non-reflective port fraction and the reflectivity of the interior surface. While most proprietary sphere coatings are in the range 95-98% the difference this variance has on surface radiance is multiplied by the sphere multiplier *M*

$$\frac{\Delta L_s}{L_s} = \frac{\Delta\rho}{\rho} * M \qquad (3.9)$$

So the increase of 3% in reflectivity can have an effect of 40-90% increase in surface radiance.

The most common pigment medium for a reflectance paint coating is Barium Sulphate. It offers >97% reflectivity over the wavelength range 400-1000nm with a relatively flat spectral profile [21].

It is the variation in this profile coupled to the *M* factor that makes careful calibration of the sphere detector system important to ensure accurate results from gathered data. Adhesion to the sphere internal surface must also be considered and suitable preparations are to be considered. Tests are to be made to ensure that any pre-treatment does not produce any unwanted fluorescence.

3.3.3 Baffles

It is important that the photo detector is not subject to direct illumination from any portion of the incident flux. This can be a problem with thin film materials due to the wave guiding effects discussed earlier. The aim is to only detect incident flux which has undergone at least two internal reflections from the sphere surface. To achieve this it is necessary to build into the sphere a baffle arrangement to make this possible fig 3.4. Baffles can be factored into any equations as an extension of the sphere surface though it is not usually considered significant [15].

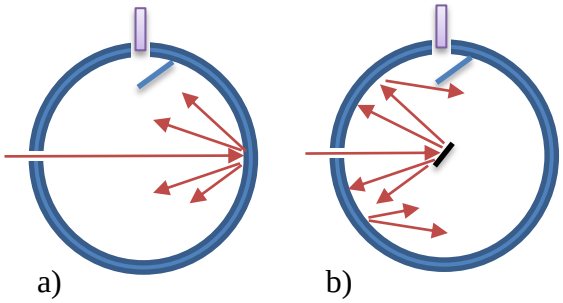

a) b)

Fig 3.4
Showing sample "out" (a) and "in" (b)

3.3.4 Fibreoptic Coupling

It has been proposed that the experiment uses an Ocean Optics USB2000 spectrometer. This gathers light using a fibreoptic cable. The incident flux gathered by such a cable when coupled to an integrating sphere is the projected solid angle.

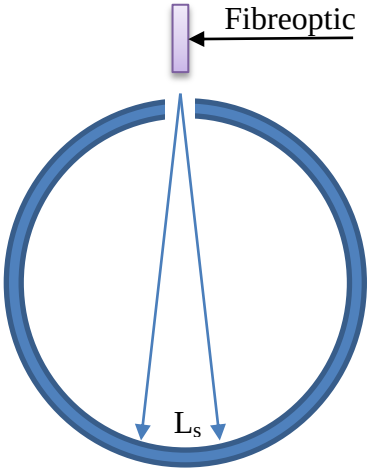

Fig 3.5

The total flux accepted by the fibre can be defined as:

$$\Theta_f = L_s A_f \pi (NA)^2 (1 - R) \quad (3.10)$$

Where A_f is the collection area of the fibreoptic tip. NA is the numerical aperture of the cable and R is the reflectance at the face of the tip.

4. Laser illumination.

4.1 Introduction

The advantages of laser illumination were described by Crosby et al as early as 1976 [13]. These include the narrow spectral line width, high power availability and a highly coherent beam of very small area.

The proposal for this project is to illuminate the samples with a heavily collimated diode laser in the wavelength of 453nm this should place the detected laser luminosity outside the range of anticipated emission from the sample materials. This substantially simplifies the calculation and extraction of luminosities for Illumination (L) and emission (E) from the gathered data. The anticipated spectra will be a combined profile of those shown in figs 2.3 and 2.4 (Fig 4.1).

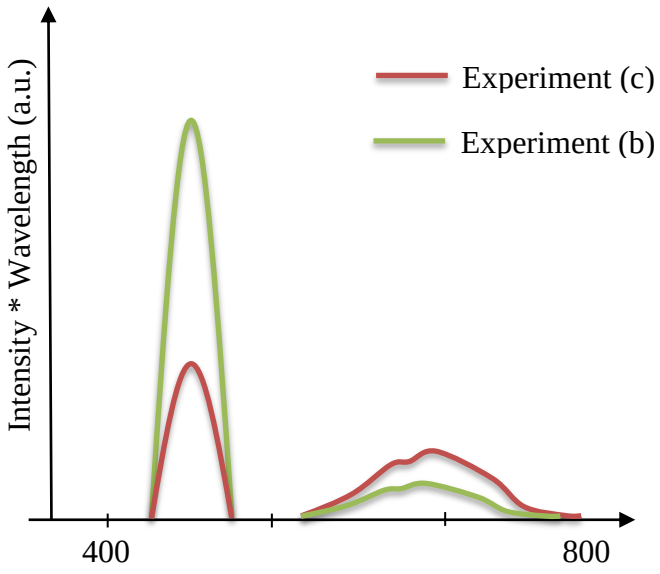

Fig 4.1

5. Calibration

5.1 Introduction.

Obtaining **relative** PLQY values for a group of individual materials is relatively straight forward as the spectrometer can plot results with the correct spectral shape and intensity scaled from 0 to 1 in arbitrary units.

To obtain accurate data for the absolute measurement of PLQY of thin film materials using an integrating sphere method, it is necessary to calibrate the system as a complete unit against a traceable light source standard. This accounts for the spectral profile of the sphere coating material, incorporating the sphere multiplier factor (*M*) along with the spectrometer instrument response function (IRF). An absolute irradiance measurement will produce a spectrum that is accurate in both shape and magnitude.

5.2 Blackbody Radiation

To calibrate the sphere detector system it is necessary to use a black-body radiation source.

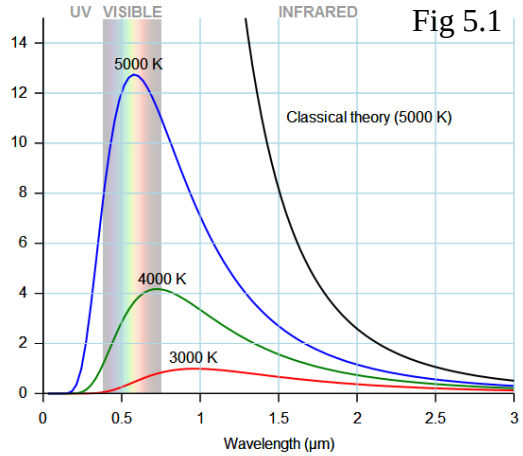

Fig 5.1

Pic Credit: D.Kule Wikimedia commons

As shown in fig 5.1, ideal black-body radiation has a continuous frequency spectrum which depends only on the temperature of the source.

A tungsten halogen lamp is a suitable blackbody source providing a continuous spectrum free from emission lines. They have good temporal stability when connected to a current regulated power supply. Such a lamp can be placed at a precisely measured distance as described by Johnson et al [11] and its light allowed to enter into the sphere through a precision aperture of known area. This will allow a

known quantity of flux into the sphere Fig 5.1.

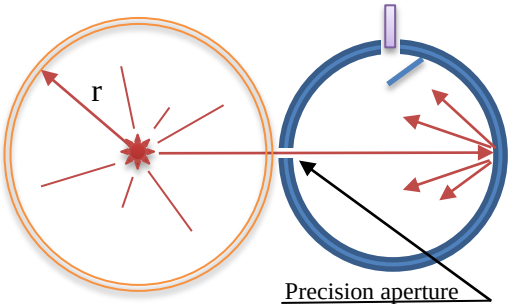

Fig 5.1

For any known photon flux $f(\lambda)$ entering or generated within the sphere, the spectral response as measured by the detector system (L_a) is the result of the geometric response of the detector $R_{de}(\lambda)$:

$$L_a = f(\lambda) * R_{de}(\lambda) \qquad (5.1)$$

Calculation of the instrument response function $R_{de}(\lambda)$ using the known irradiance of the calibration lamp over the surface of the sphere, is the ratio of detected response to known photon flux:

$$R_{de}(\lambda) = \frac{L_{std}(\lambda)}{f_{std}(\lambda)} \qquad (5.2)$$

5.3 How to calibrate.

In practical terms to calibrate an Ocean Optics Spectrometer a spectrum is measured with the sampling optic (fibre-optic and any applied correctors) connected to the calibration light source through the integrating sphere, as in fig 5.1, This is then compared to the known output power of the calibration light source. The calibration process generates a software file with energy response data for each pixel in the CCD, which is given in µJ/count. Factoring in the surface area of the sampling optic and the integration time allows irradiance measurements in µW/cm^2 to be recorded (power = energy/time). Calibration is only possible if the absolute power output of the calibration light source is known, so the light source calibration data is required in µW/cm^2/nm.

Calculation of individual absolute values is done by determination of eqn 5.3 [22]

$$L_p = C_p * \frac{S_p - D_p}{T * A * \Delta x_p} \qquad (5.3)$$

Where:

Cp = Calibration file, (µJ/count)

S_p = Sample spectrum, (counts)

D_p = Dark spectrum, (counts)

T = Integration time, (seconds)

A = Collection area, in cm^2 (A=1 for an integrating sphere)

Δx_p = Wavelength spread (how many nanometers each pixel represents)

A possible alternative, would be the use of a calibrated LED placed within the sphere, This is possible so long as the spectral range of the LED is sufficient to cover the anticipated range of results.

Once calibrated for absolute measurement it can then be possible to conduct verification using a known reference sample such as Flourescein or Rhodamine in solution, for which PLQY values are well established in literature [19].

5.5 Possible Errors and their Control.

Correct calibration is vital to ensure validity of any results so care and attention to detail is paramount. The spectrometer diffraction grating has a limited useable range depending on its groove density, this will need to be coordinated with the expected spectral range. Calibrated tungsten lamps have a finite lifetime.

6. Spectroscopy

6.1 Introduction.

The first method of spectral analysis was developed by Joseph von Fraunhoffer in the early 1800's. Spectroscopy was applied in 1859 by Bunsen and Kirchoff to chemistry and was received with great enthusiasm by William Crookes. Crookes used spectroscopy to discover the element Thallium in 1861, a previously unknown element with a bright green emission line.

For a modern Spectrometer passing the source light through an entrance slit and then directing it over a diffraction grating splits the light into spectral bands. This is then reflected onto a CCD where the count of incident photons of each specific wavelength can be integrated over time.

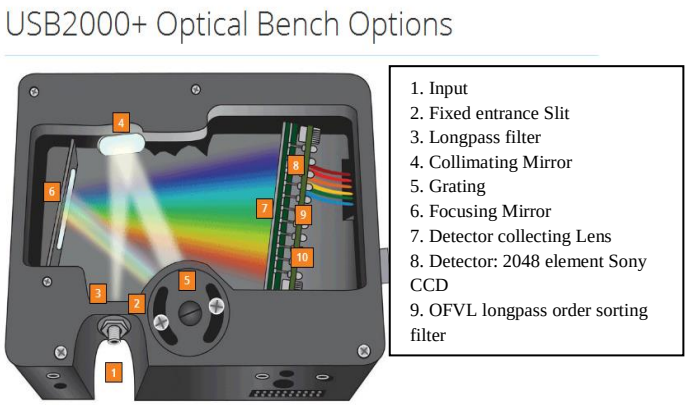

Fig 6.1. Picture Credit: Ocean Optics

6.2 Methodology

A Usb2000 spectroscope system from Ocean Optics.(fig 6.1) is the proposed instrument to gather the spectral data. It has a range of 350nm to 850nm with a resolution of 3nm (FWHM). It uses a fibre optic cable to collect the source light and direct it to the sensor.
Calibration as described in section 5 is vital for absolute measurements

7. Thin Film Technology

As described in the introduction electroluminescence is the basis for many types of visual display unit [2,4]. Conjugated polymers offer a simple yet robust structure which can be made soluble in organic solvent, this can allow high speed low cost fabrication by methods similar to screen or inkjet printing, producing a relatively large area light emitting diode display [3,4]. The advantages of this type of organic light emitting diode (OLED), over LCD or older style cathode ray displays are reduced power consumption, high contrast and low material costs. Active matrix organic light emitting diodes (AMOLED) are a further development and are currently in use on some mobile phone display devices. This uses an active matrix of OLED pixels deposited onto a thin film transistor (TFT) backing which acts as the switching mechanism to control current output to each pixel. This approach offers the possibility of even lower power consumption and with further development even lower cost.

For display devices a direct correlation has been made between PLQY and electroluminescence [9] For luminous displays high PLQY values indicate reduced energy consumption requirements. For photovoltaic cells a low PLQY material will be desirable.[3].

Visual Displays

Visual displays such as televisions and computer monitors were initially cathode ray tube (CRT) displays. Bulk size and power consumption limited any significant portable use. The development of LED /LCD has allowed a portability leading to modern smart phone and tablet computer displays. These are light, cheap and power efficient. Currently LED are in the process of being replaced by OLED technologies which have further reduced cost, thickness and energy requirements.

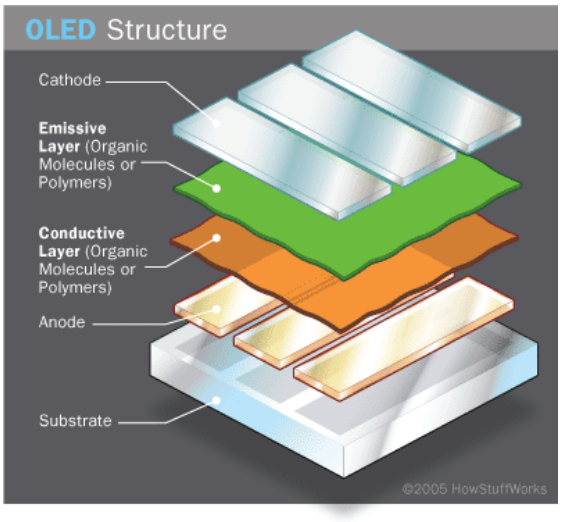

8. Conclusion

The aim of the project is to design and manufacture an experiment that is both physically and experimentally robust enough to reliably establish the absolute photo-luminescent quantum yield of some novel conjugated polymer thin film materials.
Following the method of experimental method of deMello et al [1] and using the mathematical treatment of T.Ahn et al [10] will provide results that suitably account for reabsorption and re-emission of the illuminated sample. Calibration to establish absolute values will require methods as proposed by Johnson et al [11] and reference to a certified blackbody illumination standard. The confirmation of calibration by the use of a fluorescence standard should mean that results for the novel samples have a high degree of confidence.
The design of the integrating sphere will concentrate on the guidance given by Labsphere [15,16] to ensure an optimised performance by minimising the port fraction and maximising internal reflectance, with consideration to the sample holder, baffle details and minimisation of any stray light.
Errors are to be reduced by detail consideration of influencing factors and then calculated in a manner proposed by reference to the appropriate standard [20].

Improvements over previous work.
The proposal is to use 3d printing to manufacture the integrating sphere, thereby allowing a custom design with the inclusion of specific features such as the angular control of laser-sample incidence angle to confirm the anticipated isotropic distribution within the sphere.
Additionally this approach will provide a low cost means of manufacture, potentially allowing use in undergraduate experimental teaching to reinforce concepts learnt in modules such as Optics, Optronics and semiconductor physics.

9. Acknowledgements

I would like to express thanks to Dr Chris Finlayson for guidance on technical papers and methodology. Dr Dave Langstaff for help with construction methods and guidance on experimental approach. Dr Matt Gunn for practical assistance about design and help in obtaining product guides and specification sheets.

Bibliography

[1] J.C. de Mello et al ***"An Improved Experimental Determination of External Photoluminescence Quantum Efficiency"*** Advanced Matter 9, 230 (1997)
[2] J. H. Burroughes, D. D. C. Bradley, A. R. Brown, R. N. Marks, K. Mackay, R. H. Friend, P. L. Burns† & A. B. Holmes. ***"Light-emitting diodes based on conjugated polymers"*** Nature 374 pg 539-541 Oct (1990)
[3] C. W. Tang et al ***"Two-layer organic photovoltaic cell"*** Appl. Phys. Lett. 48, 183 (1986)
[4] C. W. Tang et al ***"Organic electroluminescent diodes"*** Appl. Phys. Lett. 51, 913 (1987)
[5] N.C. Greenham a, I.D.W. Samuel a, G.R. Hayes a, R.T. Phillips a, Y.A.R.R. Kessener b, S.C. Moratti ', A.B. Holmes ', R.H. Friend (1995**)** ***"Measurement of absolute photoluminescence quantum efficiencies in conjugated polymers"*** Chemical Physics Letters 241 (1995) 89-96
[6] Laurent Porr`es, Adam Holland, Lars-Olof P°alsson, Andrew P. Monkman, Chris Kemp, and Andrew Beeby (1878). ***"Absolute Measurements of Photoluminescence Quantum Yields of Solutions Using an Integrating Sphere"***. Journal of Fluorescence, Vol. 16, No. 2, March (2006)
[7] L.Palsson, A.Monkman, ***"Measurement ofSolid-State Photoluminescence Quantum Yields of Films Using a Fluorimeter"*** Advanced Materials 14 No:10 (2002)
[8] J.Makowiecki, T.Martynski, "***Absolute photoluminescence Quantum Yield of Perylene Dye Ulltra-Thin Films"*** Organic Electronics 15 pg: 2395-2399 (2014)
[9] Z.Shuai, D.Beljonne, R.J.Silbey, J.L.Bredas ***"Single and Triplet Exciton Formation Rates in Conjugated Polymer Light-Emitting Diodes"*** Physical Review letters Vol 84 No:1 Pg 131-134 Jan (2000)
[10] T.Ahn, R.Al-Kaysi, A.Muller, K.Wentz, C.Bardeen. ***"Self-absorption correction for Solid-State photoiuminescence Quantum Yields from Integrating Sphere Measurements"*** Review of Scientific Instruments 78,086105 (2007)
[11] A.Johnson, S.Lee, J.Klein, J.Kanicki,. ***"Absolute Photoluminescence Quantum Efficiency Measurement of light-emitting Thin Films"*** Review of Scientific Instruments 78,096101 (2007)
[12] J. Campos ***"Radiometric Calibration of Charge-Coupled-device video Cameras"*** Metrologia 37, 459-464 (2000)
[13] G.Crosby, J.Demas, J.Callis ***"Absolute Quantum Efficiencies"*** Journal of Research of National Bureau of Standards. Vol.76A no:6 Dec (1972)
[14] J.Birks, ***"Fluorescence Quantum Yield Measurements"*** Journal of Research of National Bureau of Standards. Vol.80A no:3 June (1976)

[15] Labsphere Technical Guide ***"Integrating Sphere Theory and Applications"*** unpublished
[16] Labsphere Technical Guide ***"Reflectance Materials and Coatings"*** unpublished
[17] "Spectrophotometry and Spectrofluorimetry" DA.Harris & CL.Bashford IRL Press Oxford.
[18] A.Nollau, M.Hoffmann, K.Floreck, T.Fritz, K.Leo, ***"A Simple Measurement of the Absolute Internal quantum Efficiency of Thin Organic Films"*** Journal of Applied Physics Vol: 87 No: 11 pg 7802-7804 (2000)
[19] C.Wurth, M.Grabolle, J.Pauli, M.Spieles, U.Resch-Genger, ***"Comparison Methods and Achievable Uncertainties for the Relative and Absolute Measurement of Photoluminescence Quantum Yields"*** Analytical Chemistry Vol: 83 pg: 3431-3439 (2011)
[20] International organization for Standardization: Guide to Expression of Errors in Measurements (1995)
[21] Avian Technologies Data Sheet "***Avian B White Reflectance Coating***" unpublished
[22] OceanOptics Technical Note: ***"Absolute Irradiance Measurement"*** unpublished